DOI: 10.1111/imr.12687

INVITED REVIEW

WILEY Immunological Reviews

Mathematical modeling of within-host Zika virus dynamics

Katharine Best | Alan S Perelson

Theoretical Biology and Biophysics, Los Alamos National Laboratory, Los Alamos, NM, USA

Correspondence: Alan S. Perelson, Theoretical Biology and Biophysics, Los Alamos National Laboratory, Los Alamos, NM, USA (asp@lanl.gov).

Funding information
National Institutes of Health (NIH), Grant/Award Number: R01-AI028433, R01-AI078881 and R01-OD0110955

Summary

Recent Zika virus outbreaks have been associated with severe outcomes, especially during pregnancy. A great deal of effort has been put toward understanding this virus, particularly the immune mechanisms responsible for rapid viral control in the majority of infections. Identifying and understanding the key mechanisms of immune control will provide the foundation for the development of effective vaccines and antiviral therapy. Here, we outline a mathematical modeling approach for analyzing the within-host dynamics of Zika virus, and we describe how these models can be used to understand key aspects of the viral life cycle and to predict antiviral efficacy.

KEYWORDS
mathematical modeling, viral dynamics, Zika virus

1 | INTRODUCTION

Zika virus (ZIKV) is a flavivirus first isolated in Uganda in 1947[1] that is primarily transmitted between humans via a mosquito vector. Recent outbreaks in Micronesia[2] and South America[3] have suggested an association between infection, which generally manifests as a mild fever,[4] and more severe outcomes such as neural[5] and fetal[6] complications, resulting in a global effort to understand this virus more fully.

A typical ZIKV infection produces relatively rapid viral dynamics, with the median time to undetectable viremia in the blood being on the order of 2 weeks.[7,8] Not only is ZIKV detected in blood, it widely disseminates, with viral particles being detected in easily sampled compartments, such as urine,[9] semen,[10] and breast milk.[11] Understanding the rapid viral kinetics and widespread dissemination of ZIKV, including its apparent ability to cross both the blood-brain barrier[12,13] and the placental barrier[14–16] will be vital in assessing and reducing infection risks, and to evaluate the effectiveness of therapeutic interventions.

Key questions in current Zika research involve the mechanisms of immune control of infection. Vaccines are in development, as reviewed in (17,18); there is currently no safe and effective antiviral therapy and identifying and understanding key protective immune responses will be fundamental to both therapy and vaccine development.

Mathematical modeling has a long history of providing insight that would be difficult to obtain purely experimentally. Successes in modeling HIV and HCV infection and treatment[19–21] were followed by the development of models for acute viral infections such as influenza,[22–24] West Nile virus infection,[25,26] dengue virus,[27,28] Ebola virus,[29] and ZIKV.[30] Here, we review how mathematical modeling approaches can be applied to ZIKV infection.

2 | ZIKA VIRAL LOAD DYNAMICS

Viral load is a key quantity used to assess disease burden and transmission risk and understanding the longitudinal changes in viral load during infection is the focus of most within-host mathematical modeling efforts. In studies of patients presenting with symptoms of ZIKV infection, viral loads in serum have been measured (Figure 1A), showing variability in viral dynamics among patients. Different studies have found different distributions of the time to undetectable viremia. In a study of 15 infected males in Guadeloupe,[7] over 60% of patients had undetectable virus in serum by day 20 after symptom onset, while in another study involving 30 patients[31] the median time to clearance in plasma was estimated to be 11.5 days. A much larger study,[8] which recruited 150 patients, found a median time until loss of RNA detection in serum between these 2 values, at 14 days

This article is part of a series of reviews covering Modeling Viral Infection and Immunity appearing in Volume 285 of *Immunological Reviews*.

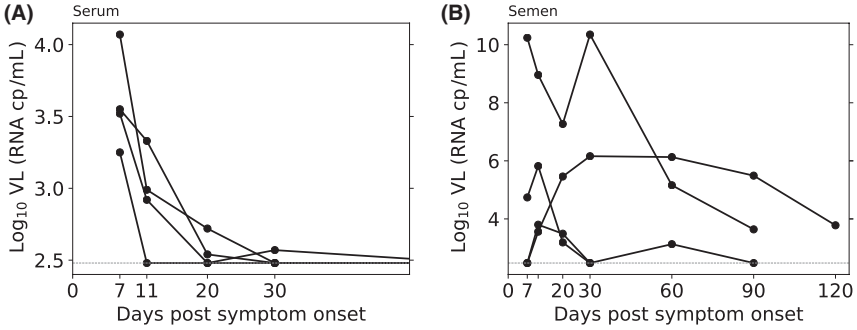

Figure 1. Zika viral infection dynamics in human patients. Zika RNA concentration in (A) serum and (B) semen from patients presenting with acute infection, data taken from Joguet et al.[7] The dashed lines represent the reported experimental limit of detection of the assays. When samples contained undetectable ZIKV they are shown at the limit of detection

after symptom onset. Additionally, viral loads in semen have been measured (Figure 1B), providing information about the duration of risk of sexual transmission and showing the presence of virus particles out to 4 months.[7] In one individual RNA was detected in semen as long as 9 months after symptom onset.[10] Given the association between ZIKV infection and birth defects, the course of infection in pregnant women has been of great interest, and sustained plasma viremia has been observed for >100 days.[32]

Using data from people infected with ZIKV presents challenges for studying viral dynamics, since only data from patients who present at clinic is available, the date of infection is generally unknown, and only the viral dynamics after onset of symptoms are available for analysis. As such, animal models are used to obtain more controlled and detailed data. In mouse models, the innate immune response generally needs to be restricted in order to obtain productive infection[33] and thus this animal model is of limited use when investigating immune control of human disease. Many groups use non-human primate (NHP) models for studying viral infection,[34] and as reviewed by Osuna and Whitney[35] and Newman et al.[36] these provide a good model for human ZIKV infection, recapitulating many of the key clinical features including acute plasma viremia that is rapidly controlled, dissemination into multiple body compartments and, when infection occurs during pregnancy, fetal pathology and prolonged viral shedding.[37] In this review we will focus on mathematical modeling of NHP viral dynamics, as a technique to aid understanding of the pathogenesis of infection and evaluating potential therapeutic approaches.

Most NHP studies use a subcutaneous challenge model, intended to mimic infection via mosquito bite. Plasma viral dynamics after subcutaneous infection show acute infection dynamics much like those found in influenza,[22] characterized by a period of exponential growth that attains a peak viral load followed by a period of exponential decline until the virus becomes undetectable (Figure 2A and B). Subcutaneous infection with a low challenge dose (Figure 2B) shows slower viral dynamics, with a later peak (Figure 2C) and generally delayed viral clearance (Figure 2D), as well as a lower peak viral load (Figure 2E) but a similar total viral burden (Figure 2F) as compared with a high-dose challenge (Figure 2A).

In addition to infection with different challenge doses, different viral strains have been used in different studies, which could well affect viral dynamics. Phenotypic differences have been observed with different viral strains with Asian strains found to be less pathogenic, having a lower infection rate, less viral production, and poorer induction of early cell death than African strains.[38]

Zika virus has been found to be able to infect a large variety of cells, including epidermal, placental, fetal, and neural cell types,[39–45] and in vivo infection studies in NHPs have found virus in many body compartments and tissues.[46] Virus has been found in semen after clearance in plasma, in agreement with human studies, thus allowing for further investigation into the risk of sexual transmission.

Zika virus infection of pregnant macaques (Figure 3A) results in prolonged maternal viremia as well as fetal pathology[37,47,48] and ZIKV infection of the fetus,[49] mimicking features of human infection. Similar results have also been found in marmosets.[50] These studies in primate models thus provide valuable data to aid understanding of the factors affecting fetal viral burden and the associated risk of severe fetal outcomes.

Plasma viral dynamics in NHPs infected via a mosquito vector (Figure 3B) were slower than in animals infected subcutaneously with 10^4 plaque-forming units (PFU) of ZIKV (Figure 2B, blue triangles), however, the peak plasma viral loads were not statistically different.[51] The delayed peak viral load may be due to the fact that the effective challenge dose provided by the feeding mosquitos was lower than that given subcutaneously, as the amount of virus in the mosquito saliva was approximately 2-3 $\log_{10}$ PFU.[51] This mosquito infection model is likely to provide essential information in comparing the highly controlled subcutaneous infection model to a more natural infection. The plasma viral dynamics following infection via mosquito demonstrates broadly similar behavior to those observed after subcutaneous infection, but with more variability between animals. A mathematical modeling approach might be able to quantify this variability. Additionally, other routes of infection have been studied in NHP models. Saliva from infected animals, despite containing viral RNA, does not appear to be capable of transmitting infection.[52] To further understanding of sexual transmission of ZIKV, vaginal, and rectal challenges have been used,[53,54] finding both routes are able to produce an infection measurable in serum (Figure 3C), with dynamics that look very comparable to the subcutaneous infection route.

3 | MODELING ACUTE VIRAL DYNAMICS

The starting point for mathematical modeling of the within-host dynamics of most viral infections, including ZIKV, is usually plasma

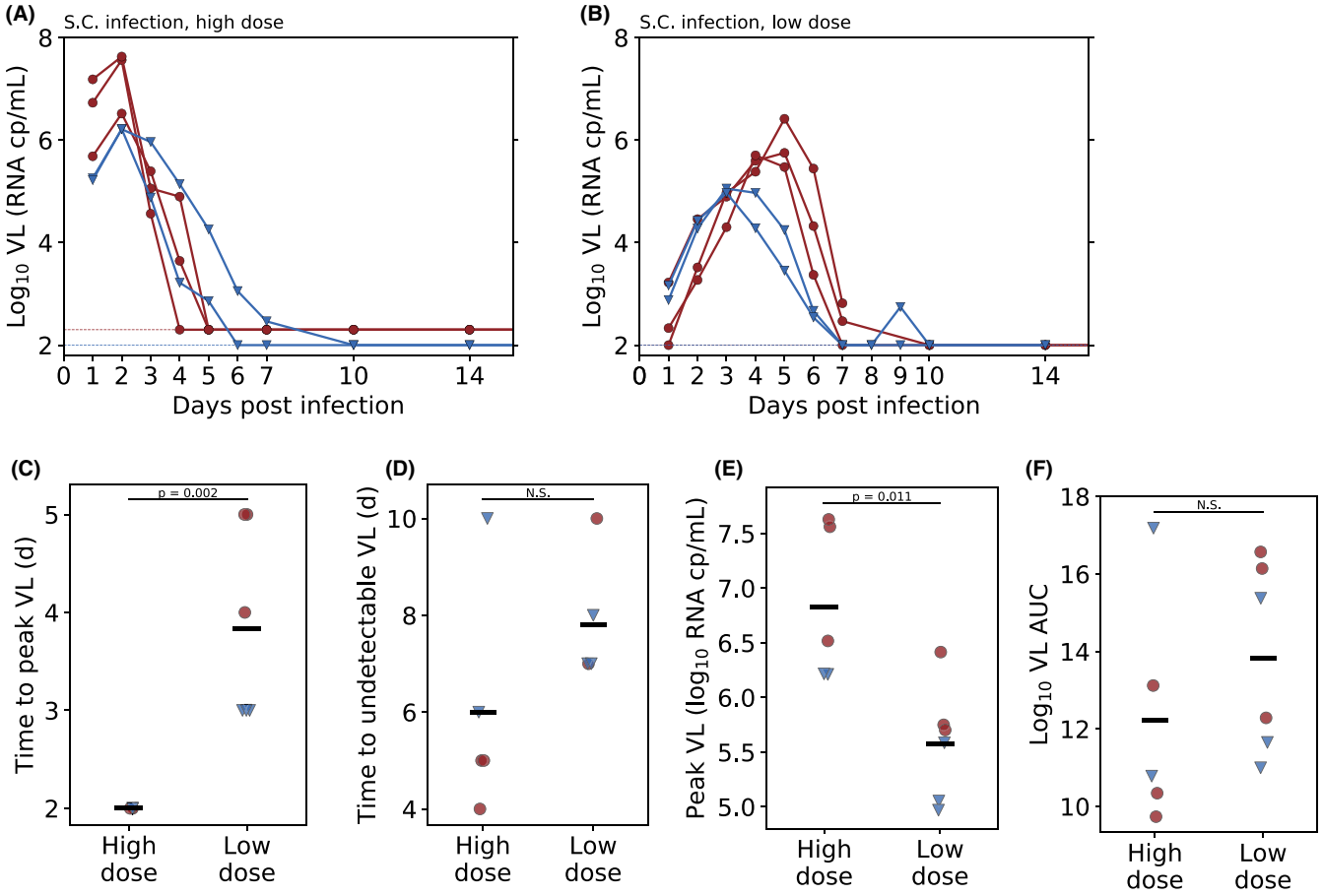

Figure 2. Zika viral infection dynamics in NHPs after high- or low-dose subcutaneous infection. ZIKV RNA concentration (A) in plasma of rhesus macaques (RM) after subcutaneous (SC) infection with a high dose of ZIKV. Red, circles: data taken from Osuna et al.,[86] after infection with 10^6 PFU of a Thai isolate of ZIKV (PLCal_ZV). Blue, triangles: data taken from Aid et al.,[116] after infection with 10^6 PFU of a Brazilian strain of ZIKV (Brazil/ZKV2015), (B) in plasma of RM after SC infection with a low dose of ZIKV. Red, circles: data taken from Aid et al.,[116] after infection with 10^3 PFU of a Brazilian strain of ZIKV (Brazil/ZKV2015). Blue, triangles: data taken from Aliota et al.,[128] after infection with 10^4 PFU of a Puerto Rican strain of ZIKV (PRVABC59). In (A) and (B) the dashed lines represent the reported experimental limit of detection of the assays. When samples contained undetectable ZIKV they are shown at the limit of detection. Summary statistics for those viral load dynamics shown in (A) and (B). (C) The time to peak viral load, (D) the time to first undetectable viral load, (E) the peak observed viral load, and (F) the area under the curve (AUC) measured between $\log_{10}$ viral load and $\log_{10}$ assay detection limited, using a trapezoidal approximation. In (C) to (F), the marker color and shape is as for the data in (A) and (B) for high dose and low dose respectively, and *p*-values shown are from a Mann–Whitney *U* test

viral loads after infection, since these data are widely available, are broadly amenable to modeling, are often used in clinical assessment and may provide information regarding key aspects of the balance between viral replication and immune control.

The exponential increase, peak viral load, and exponential decrease characterizing acute plasma viremia could be described in a phenomenological manner via the rates and timings of the growth and decline phases, but in order to gain understanding of the underlying interactions between the virus and its host a model describing how these rates are produced is required.

3.1 | Target cell-limited model

A target cell-limited ordinary differential equation (ODE) model of the following form provides a mechanistic description of plasma viral load dynamics after infection:

$$\begin{aligned}\frac{dT}{dt} &= -\beta VT\\ \frac{dI}{dt} &= \beta VT - \delta I\\ \frac{dV}{dt} &= pI - cV\end{aligned} \tag{1}$$

In this model target cells, *T*, are infected by free virus, *V*, according to a mass-action law with infection rate constant β. Infected cells, *I*, produce virus at per capita rate *p* which is cleared at rate *c* per virion. Productively infected cells die at a constant rate δ representing the known viral cytopathic effects of ZIKV infection.[55,56] This model has been used in numerous contexts to model acute viral infection, for example with influenza,[22] West Nile virus,[25] and ZIKV.[30] Estimation of model parameters for a given set of viral dynamic data is the crucial first step to allow for insight into viral replication as well as enabling prediction of the efficacy of proposed therapeutic or vaccination strategies.

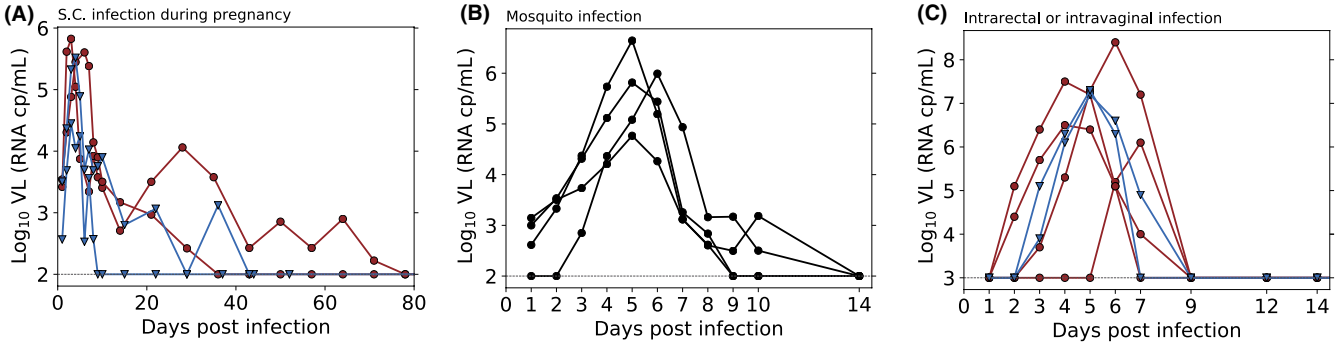

Figure 3. Zika viral infection dynamics in NHPs infected during pregnancy or by alternative infection routes. ZIKV RNA concentration (A) in plasma of RM after SC infection with 10^4 PFU of a French Polynesian strain of ZIKV while pregnant, data taken from Nguyen et al.[49] Red, circles: RM-infected mid-first trimester of pregnancy. Blue, triangles: RM-infected late-second or early-third trimester of pregnancy, (B) in plasma of RM after infection with a Puerto Rican strain of ZIKV (PRVABC59) via mosquito vector, data taken from Dudley et al.,[51] (C) in plasma of RM after intrarectal (red, circles) or intravaginal (blue, triangles) infection with 10^7 PFU of ArD 41525 ZIKV, data taken from Haddow et al.[54] In all panels, the dashed line represents the reported experimental limit of detection of the assay. When samples contained undetectable ZIKV they are shown at the limit of detection

The viral load data obtained from NHP infection models (Figure 2A and B) are amenable to individual model-fitting as well as population model-fitting approaches if data from enough animals are available. With individual fitting, a parameter set is estimated for each subject separately, allowing for the best possible model fit for each animal. Generally, the parameter set is selected to minimize the error between the model estimate and the observed data, on a $\log_{10}$ scale. For most viral load measurements there is a known limit of detection of the RNA assay, and data points which fall below this limit of detection constitute censored data. The simplest way to include censored data in the fitting procedure is to assign an error of zero if both the observation and the model prediction are below the limit of detection, and to assign an error of the difference between prediction and limit of detection if the observation is below the limit of detection while the prediction is above. A more sophisticated treatment of censored data, as presented in (57), presumes a distribution of data below the detection limit and integrates the error over this distribution.

A population fitting approach[58] takes advantage of data from multiple individuals and assumes that each parameter has a distribution of values in the population. Estimates of each of those distributions are obtained, allowing for a description of interindividual variability in each parameter. A population-fitting approach, as used in Best et al.,[30] allows for simulation of additional in-silico animals, allowing for analysis of, for instance, the predicted outcome of an antiviral therapy and the estimated number of animals that would be required in an experimental study in order to achieve enough statistical power to observe the effect of therapy.

3.2 | Basic reproductive ratio

An important concept in models of infection, whether at the epidemiological scale or the within-host scale, is the basic reproductive ratio, R_0, which represents the number of secondary infections produced by one infectious unit (person, in an epidemiological setting, or cell in a within-host setting) being introduced into a wholly susceptible population. For the target cell-limited model (Equation 1), the reproductive ratio can be derived as $R_0 = \beta p T_0/(\delta c)$,[59] and in some modeling studies the choice is made to reparametrize the model, estimating R_0 rather than β (eg Snoeck et al.[60]). We find this to be useful when estimating population distributions of parameters, allowing a description of the value of R_0 throughout the population rather than having to combine the estimated distributions of the other parameters in order to describe R_0. We have also seen that estimating R_0 instead of β tends to provide a more stable fitting procedure, and sometimes provides a better model fit,[30] as assessed by log likelihood or the Bayesian information criterion.[61] There has been concern around the possibility of ZIKV transmission via blood transfusion, and estimation of the basic reproductive ratio in vivo is of much importance in understanding the amount of time between infection and detectable plasma viral load due to its effect on the rate of exponential viral growth.[59] A recent screening study of the U.S. blood supply[62] found there to be very low risk of transmission via blood transfusion, although this is likely to be increased in countries with a higher incidence of ZIKV infection.

3.3 | Parameter identifiability and constraints

Whichever fitting method is chosen, it is important to be aware of constraints around identifying all the model parameters. In this model, fitted solely to viral load data, the parameter p and the initial condition $T(0)$ are only identifiable as the product $pT(0)$.[63,64] We generally choose to fix $T(0)$, the number of initial target cells, and estimate a value for the viral production rate p. Under this framework, it is important to remember that any interpretation of the estimated parameter p is entirely dependent on the fixed value of $T(0)$. An additional constraint on parameter values is found in the burst size, p/δ, which is the average number of virions produced by an infected cell during its productive lifetime. Since the reproductive ratio, R_0, is the number of secondary infections produced by one infected cell when target cells are not limiting, the model requires that p/δ virions are able to infect R_0 cells. Experimental estimates find that the ratio of RNA (virions) to PFU, that is, infectious particles,

is between 500 and 1000,[65] giving a limitation that p/δ > (RNA/PFU)R_0. Additionally, care needs to be given to the practical identifiability of model parameters given the available data, as discussed for example by Miao et al.,[63] Guedj et al.[66] and Nguyen et al.[67]

3.4 | Modeling the delay between infection and production

In the model described by Equation 1 newly infected cells start producing virus at rate p immediately upon infection. However, a number of stages of the viral life cycle are required to occur before viral production can actually occur and as such there will be a delay between infection of the target cell and new viral production. This delay can be incorporated in the model by splitting the infected cell compartment, I, into 2 separate compartments: I_1, for cells which are infected but not yet producing virus and I_2, for cells which are producing viral particles.[22] The period of time before infected cells start producing virus is referred to as the eclipse phase since the presence of these cells cannot be observed in the viral load data.

The amount of time that cells spend in the eclipse phase determines the form of the equation describing the rate of change of I_1. A commonly made assumption is that transition from I_1 to I_2 occurs at rate kI_1, where k is a constant.[22,30,68,69] This is equivalent to assuming the amount of time it takes before an infected cell starts producing virus is exponentially distributed, giving a model in which the single ODE for I and the ODE for V in Equation 1 is replaced by

$$\begin{aligned}\frac{dI_1}{dt} &= \beta VT - kI_1\\ \frac{dI_2}{dt} &= kI_1 - \delta I_2\\ \frac{dV}{dt} &= pI_2 - cV\end{aligned} \tag{2}$$

In this model, the average time spent in the eclipse phase is $1/k$. The model described by these equations assumes that there is no cell death while in the eclipse phase and results in an expression for R_0 equal to that for the model in Equation 1, although the time of target cells becoming productively infected is altered. In many circumstances the assumption of no cell death in the eclipse phase appears reasonable, since while viral particles are not being produced there are likely to be minimal cytopathic effects. However, if cell death, at rate δ_1, occurs during eclipse phase then the equation for I_1 becomes

$$\frac{dI_1}{dt} = \beta VT - kI_1 - \delta_1 I_1 \tag{3}$$

Furthermore, the expression for the basic reproductive ratio becomes $R_0 = \left(\frac{p\beta T_0}{\delta c}\right)\frac{k}{k+\delta_1}$, with the additional term describing the fraction of I_1 cells that survive the eclipse phase to become productively infected.[70] Incorporating a rate of cell death during the eclipse phase is supported in the case of HIV infection, where it is known that protein from infecting virus can be presented on MHC-1 molecules before the cell begins producing new virions.[71] Therefore, the immune system is able to recognize and attack HIV-infected cells while they are still in the eclipse phase. Whether this is a mechanism that also exists in ZIKV-infected cells is currently unknown, and if the length of the eclipse phase is fairly short it appears reasonable to ignore cell death during the eclipse phase.

The assumption of an exponentially distributed eclipse phase (Figure 4A, black) does not need to be made for modeling purposes, nor is it an experimentally validated assumption: it is simply the most straightforward. Careful and detailed in vitro influenza[72] and SHIV[73] infection experiments provide support for non-exponentially distributed eclipse phases, finding that a gamma-distributed time to productive infection describes the observed data far more accurately than an exponential distribution. A gamma distribution with an integer shape parameter, an Erlang distribution, for the time spent in the eclipse phase can be easily described as a series of ODEs[74]:

$$\begin{aligned}\frac{dT}{dt} &= -\beta VT\\ \frac{dE_1}{dt} &= \beta VT - knE_1\\ \frac{dE_i}{dt} &= kn(E_{i-1} - E_i) \quad \text{for } i = 2 \ldots n\\ \frac{dI_2}{dt} &= knE_n - \delta I_2\\ \frac{dV}{dt} &= pI_2 - cV\end{aligned} \tag{4}$$

where cells in compartments E_1, ..., E_n are in the eclipse phase, and the sum of the exponential distributions (the time spent in each compartment E_1 to E_n) provides a gamma distribution with integer shape parameter n, an Erlang distribution (Figure 4A, green). An Erlang distributed eclipse phase has been used in mathematical modeling studies of influenza[75–77] and HIV[74] infection, although it should be noted that use of the Erlang distribution introduces an additional parameter and therefore despite potentially describing the biological processes more realistically might not be justified by model selection criteria. As the integer shape parameter n tends to infinity, the distribution becomes tighter and tends toward a point distribution that is a fixed length eclipse phase (Figure 4A, blue), exactly equal for all cells. A model wherein all cells spend a fixed amount of time τ (= $1/k$) in the eclipse phase has been used for modeling HIV[78] as well as influenza[79] and can be described using delay differential equations:

$$\begin{aligned}\frac{dT}{dt} &= -\beta VT\\ \frac{dI_1}{dt} &= \beta VT - I_1(t-\tau) - \delta_1 I_1\\ \frac{dI_2}{dt} &= I_1(t-\tau) - \delta I_2\\ \frac{dV}{dt} &= pI_2 - cV\end{aligned} \tag{5}$$

where we set $\delta_1 = 0$ if we assume there is no cell death during the eclipse phase. In this model with a fixed length eclipse phase the increase in I_2 due to infection events only depends on the concentration of target cells and of virus at time $t - \tau$, meaning that the ODE for I_1 can be omitted[78]:

$$\begin{aligned}\frac{dT}{dt} &= -\beta VT\\ \frac{dI_2}{dt} &= \beta V(t-\tau)T(t-\tau)e^{-\delta_1\tau} - \delta I_2\\ \frac{dV}{dt} &= pI_2 - cV\end{aligned} \tag{6}$$

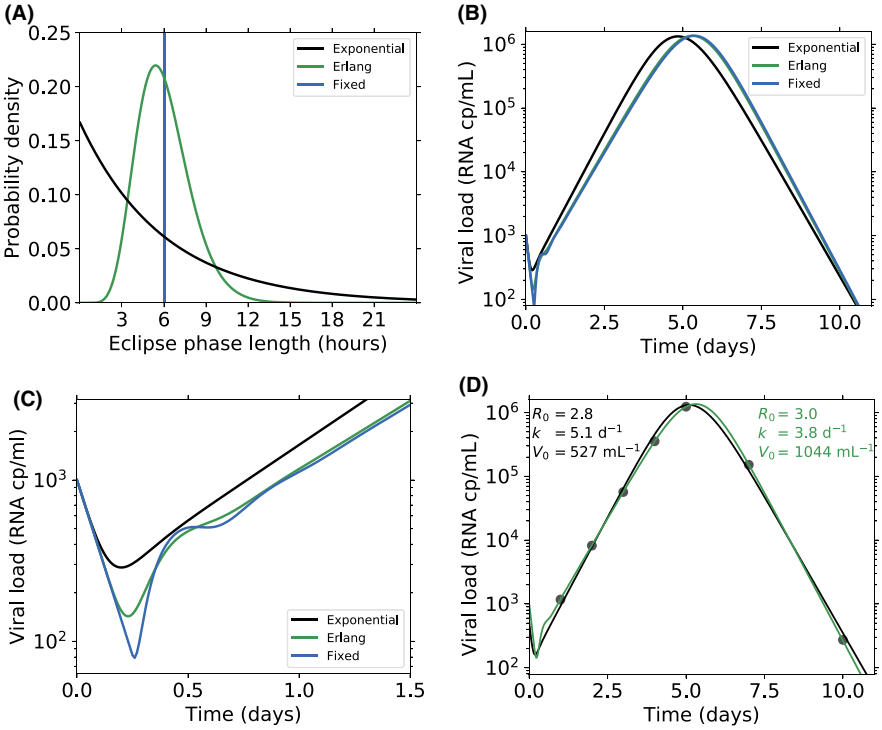

Figure 4. The distribution used to describe the eclipse phase length affects the predicted viral dynamics. (A) Eclipse phase distributions, each with an average eclipse phase length of 6 hours (eclipse phase parameter k = 4 per day, shape parameter n = 10 for the Erlang distributed eclipse phase). (B and C) Viral load given by the target cell-limited model including an eclipse phase distributed as (A), assuming no cell death occurs within the eclipse phase. The difference between using a fixed eclipse phase length and the Erlang distributed length cannot be observed on a long timescale (B) but can be seen on a short timescale (C). The viral dynamics model parameters used were R_0 = 3, k = 4 per day, δ = 3.5 per day, p = 1000 per day, c = 10 per day, $T(0) = 10^5$ per mL, and $V(0) = 10^3$ per mL. (D) Simulated "observations," using a standard NHP sampling schedule, were selected from the model with Erlang distributed eclipse phase (gray circles), and model fitting to estimate values of parameters R_0, k, and $V(0)$ for both the exponential eclipse phase model (black) and Erlang eclipse phase model (green) was performed. Other parameters were fixed at their simulation values, above

where the exponential term in the I_2 equation is the probability that an infected cell survives the eclipse phase. Under this model, the basic reproductive ratio is $R_0 = \left(\frac{p\beta T_0}{\delta c}\right) e^{-\delta_1 \tau}$.[70]

The choice of the eclipse phase length distribution affects the viral dynamics in this model. Taking different eclipse phase distributions (Figure 4A) each with an average eclipse phase length of 6 hours, since ZIKV production has been observed by 6 hours after infection in an in vitro setting,[39] and holding all other viral kinetic parameters constant, we see that the viral dynamics (Figure 4B) are altered somewhat. The main differences are seen in the early stages of infection (Figure 4C) where the non-exponentially distributed eclipse phases give a deeper initial decline in plasma viral load, and a shallower upslope, resulting in a later peak viral load. We note that viral load observations from the Erlang eclipse phase model simulation shown in Figure 4B can be well fit by both the exponential and Erlang eclipse phase models (Figure 4D), and different parameter estimates are obtained. As such, experiments employing much more frequent sampling of NHPs postinfection will be needed to distinguish between eclipse phase models.

The viral dynamics with a fixed length eclipse phase, and to a lesser extent with an Erlang distributed eclipse phase when the shape parameter n is relatively large, produce oscillatory behavior in the viral dynamics in early infection. This behavior is due to the fairly synchronized time at which the cells initially infected by the inoculum dose start to produce new viral particles. The virus produced by this first tranche of infected cells goes on to infect more target cells, although in a less synchronized manner, and the oscillations are dampened as the process continues. For the same reason, early oscillations were seen by Mitchell et al.[79] in the solution to their influenza model using a fixed length eclipse phase. The oscillatory behavior is less marked with the Erlang distributed eclipse phase since the times at which the first infected cells start producing virus is not uniform, and the behavior does not occur with the exponentially distributed eclipse phase because the infected cells are presumed to begin producing virus over a wide range of times after infection.

Mathematical modeling studies of acute viremia are most frequently based on viral load measured in the peripheral circulation, since these measurements are easily accessible, allowing for regular sampling. However, it is likely that active viral replication occurs in other anatomic compartments, and what is being observed is a combination of virus being produced in blood and virus transported into the blood from other compartments. This complexity can be

managed by considering the circulating viral load as a proxy for the total body viral burden, and the model parameters as effective rates that incorporate processes occurring in tissue plus transport to the circulation. This type of approach has been successful in modeling hepatitis C virus (HCV) infection, which is largely restricted to the liver but with viral loads measured in blood.[20] More mechanistically, a multi-compartment model could be developed that includes a tissue compartment, where active viral replication occurs, and a blood compartment, where some of the processes in the viral dynamics model occur, at a minimum viral clearance, and from which samples are taken. However, this extended model involves additional parameters and as such requires more data to reliably estimate parameter values. A multi-compartment model of this type could also be used to describe maternal viral loads in pregnancy, assuming the fetus acts as an immune-privileged reservoir, in which viral replication can continue for a prolonged period with transport back into the maternal circulation. A similar model could also be applied to infection occurring in the nervous system with viral transport back into the circulation.

A model describing viral transport between multiple anatomical compartments could also be used to more fully describe the relationship between the inoculum dose and the plasma viral load. On subcutaneous infection, the inoculum dose is deposited in tissue where it must traffic into the circulation before being observable. As such, in a single anatomical compartment model, as in Equations (1)-(6), the initial viral load $V(0)$ is presumably related to, but not equal to, the challenge dose. In its simplest form, a multi-compartment model accounting for a tissue infection site without any active replication would incorporate an additional ODE for the amount of virus at the infection site, ν, of the form

$$\frac{d\nu}{dt} = -c_t\nu - a\nu \tag{7}$$

where $\nu(0)$ is set equal to the challenge dose, c_t is the viral clearance rate in the tissue, and a is the transport rate from the infection site to the circulation. The ODE for the observed plasma viral load in Equation 1 would have an additional term, becoming

$$\frac{dV}{dt} = \frac{a\nu}{vol} + pI - cV \tag{8}$$

where vol is the volume of distribution of the virus once it reaches the circulation. The ODE for the amount of virus at the infection site (Equation 7) has the explicit solution

$$\nu(t) = \nu(0)e^{-(c_t+a)t} \tag{9}$$

where the initial condition $\nu(0)$ is the challenge dose, assumed to be known. Now the ODE for the plasma viral load (Equation 8) can be written as

$$\frac{dV}{dt} = a'De^{-bt} + pI - cV \tag{10}$$

with initial condition $V(0) = 0$, by setting $a' = a/vol$, $b = c_t + a$ and defining D as the challenge dose. In this formulation it can be seen that the infection site transport model eliminates the unknown initial plasma viral concentration and therefore only increases the number of unknown parameters by one.

4 | MODELING IMMUNE CONTROL OF VIREMIA

The model given by Equation 1 and the eclipse phase extensions described above rely on the decreasing number of available target cells as infection progresses to provide resolution of infection. After some time, the target cell population becomes low enough that the number of new infections, and therefore the number of infected cells, does not produce enough new viral particles to outpace viral clearance, hence leading to resolution of infection. In the model in Equation 1 there is no replenishment of target cells, as is considered reasonable in many cases given the short timescale of the acute infection,[22] and hence once the viral load begins to decline due to target cell loss there is no possibility of further viral growth.

In some viral infections, the assumption that target cells become limited does not appear to be directly justified. For example, a wide variety of cells are able to become productively infected when exposed to ZIKV,[39–45] and as such is it hard to imagine that target cell availability (in terms of death of cells) is primarily responsible for viral control. However, the assumption of target cell limitation can be thought of as a simplification of the model whereby some cells that are in principle susceptible to infection are protected, either spatially or via an immune response. Under this interpretation, the target cell population in the model can be considered to be those cells that are both susceptible and available for infection.

However, it is both more informative and more accurate to attempt to describe the immune effects controlling viral burden directly in the mathematical model. The general approach to incorporating immune responses in a viral dynamic model is to include those immune system cells and molecules that one suspects are restricting infection. For ZIKV infection in humans, there is currently a paucity of clear data on which immune responses are most important for viral control.

4.1 | Innate responses in ZIKV infection

In ZIKV infection, both innate and adaptive responses have been shown to be important for viral control in various experimental models. In order to obtain productive infection in adult mice, type I interferon (IFN) responses generally need to be knocked out.[33] Similarly, wildtype neonatal mice who possess undeveloped immune systems are able to be infected,[80] with pathogenesis being both dose and age dependent. In humans, ZIKV is able to suppress the type I IFN response by targeting the transcriptional activator STAT2 for proteasomal degradation, but this does not occur in mice, which may explain the requirement of knocking out the IFN response in mice to generate productive infection.[81] ZIKV has also been shown to be able to avoid the host NK cell cytotoxic response by causing

upregulation of MHC class I molecules, an NK cell inhibitor, on the surface of infected cells in vitro.[82]

4.2 | Adaptive immune responses and antibody-mediated protection

There has also been much effort directed toward understanding the generation and protective capacity of anti-ZIKV antibodies, as reviewed in Priyamvada et al.[83] In macaque models, after a high-dose intravenous infection, total numbers of B cells increased on day 3, while antigen-specific IgG titers were not detectable until well after clearance of the plasma virus, suggesting that the antibody response was more important for long-term protection than short-term control.[84] The long-term protective role of antibodies in ZIKV infection is supported by work from a number of groups.[85,86] Aliota et al.[85] found that rhesus macaques were protected from secondary homologous and heterologous challenge 70 days after primary infection. Secondary challenge produced no detectable virus in plasma, urine, and semen, although neutralizing antibodies were increased after secondary challenge, suggesting that some low-level viral replication occurred but that the animals were protected from disease. Similarly Osuna et al.[86] saw protection from secondary heterologous challenge 45 days after primary infection. A secondary heterologous challenge of a marmoset[87] 12 months after primary challenge also produced no detectable viremia but increased antibody titers were observed, demonstrating the ability of ZIKV antibody protection to persist longer term.

In humans, virus-specific antibodies are seen to develop as early as 3 days after the onset of fever,[88] although in some studies IgM was not detectable until 8 days after symptom onset[9] with IgG developing even later in flavivirus-naive patients.[31] Cross-reactivity between ZIKV and antibodies to dengue virus[89] has been observed, complicating both ZIKV diagnosis and assessment of vaccine-induced immunity.[90] This cross-reactivity means that concerns around antibody-dependent enhancement (ADE) leading to severe disease on repeated dengue infections[91] are also present with Zika infection, and in vitro studies have demonstrated the ability of dengue antibodies to drive Zika ADE.[92] However, in NHP infection models, no evidence has been found for prior flavivirus infection worsening ZIKV infection[93,94] and there is some suggestion that prior dengue exposure may even be beneficial in Zika infection, since a cross-reactive dengue antibody has been shown to be protective against ZIKV infection in mice.[95]

T-cell responses have also been shown to be capable of providing protection against ZIKV infection. In immunocompetent mice infected with ZIKV, a T cell response is seen by 7 days postinfection, with antigen-specific IFNγ-producing CD8 T cells generated.[96] These CD8 T cells, on transfer to IFNα receptor knockout mice, protect from weight loss and reduce ZIKV burden after infection. Additionally, depletion of CD8 T cells results in higher viremia in mice.[97] However, despite this evidence of T-cell response to ZIKV infection in mice, in rhesus macaques populations of CD8+ T cell subsets remain mostly stable during the course of infection.[84]

In the situation where the immune responses that should be incorporated into models are broadly unknown, each potential response can be modeled and tested via data-fitting in order to suggest areas for further experimental focus. There are a number of feasible mechanisms of immune control of viremia, each of which can be implemented in the ODE models described by Equations (1)-(6) as we discuss below.

4.3 | Innate immune response models

It is known that for some viruses host type I IFN production, in response to viral infection, is able to put some cells into a protected or "antiviral" state[98,99] and thus reduce their susceptibility to infection. Type I IFN can also reduce the rate of viral production from infected cells as has been shown in the case of HCV.[20] This innate immune response can be modeled via an additional ODE describing the production of IFN from productively infected cells, at some rate and usually after some delay[22]:

$$\frac{dX}{dt} = sI_2(t-\tau) - \alpha X \tag{11}$$

where X denotes the concentration of IFN present, s is the IFN production rate per infected cell which can be set to 1 without loss of generality (although this results in X being measured in arbitrary units), τ is the length of the time it takes for IFN to be produced and able to act, and α is the rate of IFN degradation and loss due to cell uptake.

The effect of IFN on different aspects of the viral dynamics system can then be incorporated into the model using the value of X. In Pawelek et al.,[100] IFN-induced protection of target cells was modeled as

$$\begin{aligned}\frac{dT}{dt} &= -\beta VT - \phi XT + \rho P \\ \frac{dP}{dt} &= \phi XT - \rho P\end{aligned} \tag{12}$$

where P denotes "protected" cells which are unable to be infected. These are produced via interaction between IFN, X, and target cells, T, with rate ϕ, and cells lose their protection at rate ρ. In this model, the target cell concentration initially drops rapidly (Figure 5B, orange), which is followed by a reduction in the plasma viral load (Figure 5A, orange) earlier than would be observed without IFN-mediated target cell protection. The decrease in the viral load results in a waning of the IFN response (Figure 5C, orange), which allows for an increase in target cell concentration as protection is lost and a resulting recrudescence of plasma viral load. Saenz et al.[101] introduce a more complex model with partially protected cells that ultimately transition to fully protected cells. Alternatively, a model similar to that given by Equation 12 but with the ϕXT terms replaced by $\phi XT/(X+\Theta)$ where Θ is a constant could also be used (V. Madelain and J. Guedj, private communication). In this formulation, ϕ is then the maximum rate at which a cell can become protected.

If the effect of the IFN response is modeled as a reduction in the viral infectivity, the ODEs for the target cell and eclipse phase populations become

$$\frac{dT}{dt} = -\frac{\beta}{1+\gamma X}VT$$
$$\frac{dI_1}{dt} = \frac{\beta}{1+\gamma X}VT - kI_1 \quad (13)$$

where γ is a parameter describing the strength of the immune effect. With this model the plasma viremia is reduced without the "loss" of target cells (Figure 5, green), as these cells are not transformed into protected cells as in the model given by Equation 12.

The antiviral effect of IFN can also be modeled as a reduction in the viral production rate from infected cells,[22] giving

$$\frac{dV}{dt} = \frac{p}{1+\gamma X}I_2 - cV \quad (14)$$

where again γ describes the strength of the immune effect, with this model providing a similar pattern of early reduction of plasma viral load followed by recrudescence as the innate immune response wanes (Figure 5, purple).

Innate immune responses can also result in a cytolytic effect, with the death rate of infected cells being increased as an immune response is activated. In an innate immune setting, NK cells can be activated due to presence of virus and infected cells and the level of NK cells could be described using the same form of ODE as in Equation 11. NK cells, X, then act to increase the death rate of productively infected cells:

$$\frac{dI_2}{dt} = kI_1 - \delta(1+\gamma X)I_2 \quad (15)$$

with parameter γ representing the per-interaction killing rate of NK cells. This model provides similar patterns of viral dynamics as the other innate immune models described above (Figure 5, blue).

The examples of the dynamics from each of these models (Figure 5), all demonstrate the same pattern: an innate immune response is able to control plasma viremia more rapidly than the target cell limited model, but also allows for viral recrudescence after the immune response wanes due to viral load reduction. Since any of these immune responses reduces viral load, fewer target cells become infected. Therefore, when the immune response wanes, due to lack of infected cells to produce IFN or to activate NK cells, a large proportion of the initial susceptible target cells are available to be infected by the small amount of virus that remains in the system and viremia can grow, until it is again controlled by the immune response.

We do not see this viral recrudescence in the viral loads from acute infections in NHPs. Using an ODE model structure in which variables are real numbers rather than integers there is no possibility of complete extinction of the virus, while in reality at low copy numbers there is a probability that the last infected cell dies and the last virus particle is cleared before infecting a new target cell so that the viral infection is eradicated. One can artificially introduce a threshold value for virus and infected cells below which one declares the infection cleared. Such cure boundaries have been successfully used to predict the duration of treatment needed to cure HCV.[60,102,103] Another possibility is that by the time an innate immune response wanes in effectiveness enough to allow for growth of virus, an adaptive response has been initiated to fully clear the infection and provide protection from reinfection.[100]

An interesting aspect of the innate immune model examples (Figure 5) is that under similar parameter regimes the immune mechanisms give different timings of viral control and recrudescence. This is due to the "degree of separation" between the aspect of the viral life cycle being modulated by immune control and the observed viral dynamics. A model in which the immune response restricts viral production (Equation 14, Figure 5 purple) has a very rapid impact on the observed viral loads, resulting in the lowest initial peak viral load and early control. In contrast, viral control in a model where the immune response restricts viral infectivity (Equation 13, Figure 5 green) can only be observed in plasma viral load after a full cycle of infection, eclipse phase, and viral production has occurred, demonstrated by a higher initial peak viral load and slower viral control.

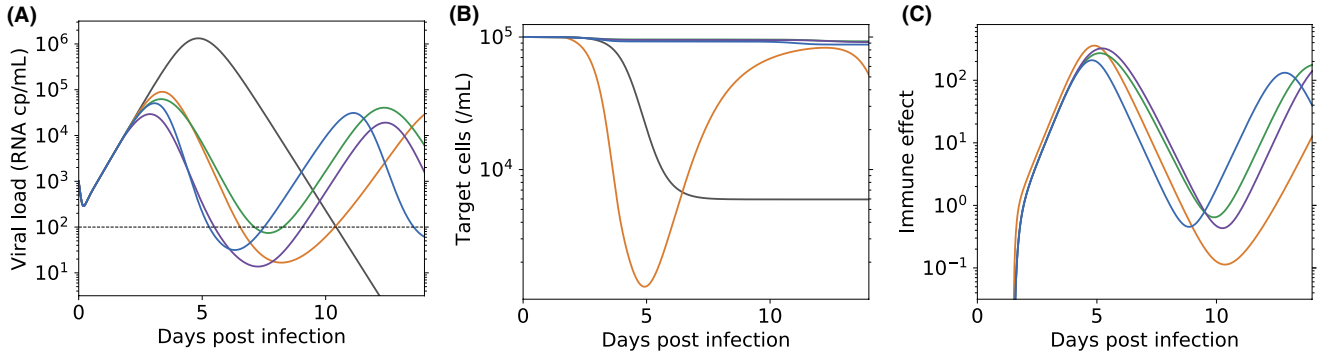

Figure 5. Viral dynamics in models incorporating an innate immune effect. For the target cell limited model (gray, Equation 2) and models incorporating innate immune effects (orange: IFN-mediated protection of target cells, Equation 12; green: IFN-mediated restriction of viral infectivity, Equation 13; purple: IFN-mediated restriction of viral production from infected cells, Equation 12; blue: NK cell-mediated cytolysis of infected cells, Equation 15), (A) viral load, $V(t)$ (B) target cell, $T(t)$ and (c) immune effect, $X(t)$, dynamics, using parameters $R_0 = 3$, $k = 4$ per day, $\delta = 3.5$ per day, $p = 1000$ per day, $c = 10$ per day, $T(0) = 10^5$ per mL and $V(0) = 10^3$ per mL, $\gamma = 0.1$ per day, $\alpha = 2$ per day, $\tau = 1.5$ day, $s = 1$, $\varphi = 0.1$ per day and $\rho = 0.5$ per day. Note that even in the target cell limited model, target cell depletion is not complete. Furthermore, in the IFN-mediated cell protection model cells that were protected by IFN return to being targets as the IFN concentration wanes beginning on day 5 (orange curve in panel (B))

4.4 | Adaptive immune response models

An adaptive cytolytic immune response, for example, via CD8+ T cells, requires a different form of model from the innate responses, due to the different mechanism of activation of effector cells. Various models have been used to describe the size of the CD8+ response, and which is most appropriate or accurate can only be ascertained when good data is collected on activated T cells during a ZIKV infection. In an influenza model developed by Handel et al.,[104] initial B- or T-cell activation was presumed to be dependent on the density of virus (and therefore antigen) present, while subsequent clonal expansion of activated cells was presumed to be antigen-independent, giving rise to the following equation:

$$\frac{dX}{dt} = fV + rX \tag{16}$$

where f and r are rate constants. Other models[105,106] allow for effector cell expansion only when there is interaction with infected cells, and introduce a term to ensure this expansion saturates, yielding

$$\frac{dX}{dt} = rX\frac{I}{I+\kappa} - \alpha X \tag{17}$$

where κ is a "carrying capacity" and α is the death or deactivation rate of activated CD8+ cells. Immune exhaustion can be modeled by including an additional negative term in this expression,[105,107] but at the cost of added complexity and additional model parameters. Models of the CD8 T-cell response during acute lymphocytic choriomeningitis virus infection of mice have been developed that not only include effector cell expansion, but also a contraction phase after viral control has been established as well as the formation of immune memory.[108,109] Such models might be applicable to ZIKV infection. Lastly, the effect of cytolytic CD8+ T cells is usually included in the model by adding a mass-action term of the form $-\gamma XI$ to the productively infected cell equation.

The effect of antibody, A, is often modeled for other viral infections in a similar way, but now as a mass-action term clearing free virus,[104,110] i.e.,

$$\frac{dV}{dt} - pI_2 - cV - \gamma VA \tag{18}$$

while assuming either that the antibody concentration follows the B-cell concentration, as described by Equation 16 or invoking a more detailed model of antibody production.[111–113] Antibody can also have other effects. For example, if the antibody is neutralizing then it will reduce the rate of infection, which can be modeled by Equation 13, where X is now interpreted as the neutralizing antibody concentration rather than the IFN concentration.[114] By binding to infected cells, antibody can increase their rate of cell death by fixing complement, by activating the cytotoxic effect of NK cells in a process called antibody-dependent cellular cytotoxicity, and by opsonizing the cell and increasing the rate of infected cell phagocytosis, a process called antibody-dependent cellular phagocytosis. A simple way to model any of these processes is to use Equation 15 where X is interpreted as the antibody concentration.[114]

Which of these models of immune control of viremia is most appropriate to apply to ZIKV is not obvious. In Osuna et al.[86] a wide range of immune cell subsets and cytokines were measured during acute ZIKV infection. In order to determine which may be important for viral control, and therefore which should be included in models, we performed a number of correlation analyses looking to see if an increase in any immune parameter correlated with a decrease in virus.[30] After correcting for multiple testing, none of our analyses revealed a strong signal of a mechanism of immune control. We also saw that the dynamics of the changes in IFN concentration and levels of NK cells and CD8 effector effects observed after ZIKV infection, and shown in Figure 6, were not readily described by any of the generally used models of immune response discussed above (Equations 11, 16, 17) and illustrated in Figure 5C. In particular, the IFNα response showed an early peak in most, but not all, animals, but this waned in many animals before the plasma viremia was controlled, and continued to increase in some animals after plasma viral load became undetectable.[30] Due to this, we were not able to use a viral dynamics model incorporating a simple model of immune response to fit these data.[30] Interestingly, we also observed that the immune dynamics were much more varied between animals than the plasma viral dynamics. This high level of heterogeneity in immune dynamics resulting in little heterogeneity in viral dynamics perhaps

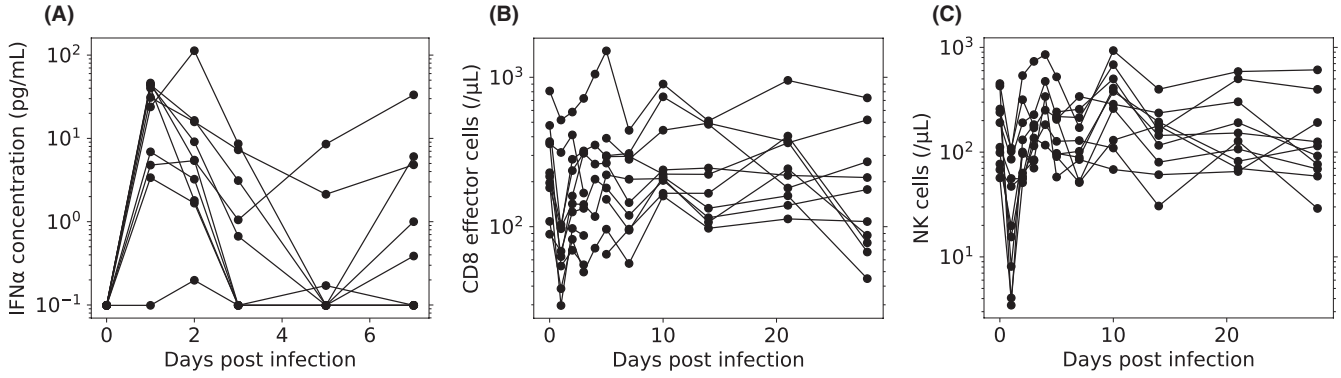

Figure 6. Measured immune dynamics during ZIKV infection of rhesus macaques. Data from Best et al.[30] and Osuna et al.[86] Measured (A) IFNα, (B) CD8 effector cell and (C) NK cell concentrations after subcutaneous infection with 10^6 PFU Thai strain ZIKV

indicates either that target cell limitation is the predominant factor or that multiple immune responses contribute to viral control, allowing variability in individual immune responses to have little impact on the overall outcome in the plasma viremia.

When measured immune responses are not well-fit by simple ODE models describing immune dynamics (Figures 5C and 6), one can incorporate the immune response data into the viral dynamics model using some form of interpolation between measured values of the quantities of interest, for example, immune cell populations and cytokine levels, rather than using a poor model fit. After adopting this approach, we found that model fits incorporating immune system effects were generally indistinguishable from those using the simple target cell limited model, with or without an eclipse phase, that is, Equations (1) or (2). Thus, using measured immune data such as shown in Figure 6 we were still unable to find statistical support for any viral dynamics model incorporating immune control in fitting the viral load data presented in (30,86). This is possibly attributable to the high viral challenge dose of 10^6 PFU and the subsequent rapid viral dynamics seen in this study.

The question of the appropriate challenge dose to use in animal models, in order to most accurately model the dynamics of natural infection or to extract most information regarding the immune response, is still open. The saliva of infected mosquitos has been found to contain 2-3 $\log_{10}$ PFU of ZIKV,[51] or on average 5-6 $\log_{10}$ RNA copies.[115] Low subcutaneous inoculum doses are associated with delayed and prolonged viremia[116] but no substantial host gene transcriptomic clustering by dose was observed over a 3 $\log_{10}$ dose range. A full analysis of the limited data available on the effects of inoculum dose on ZIKV viral load has not yet been published, but analyses of data from adenovirus infection of cotton rats and infectious bronchitis virus infection of chickens found a correlation between inoculum dose and both time to peak viral load and duration of infection.[117] Furthermore, this study found that mathematical models incorporating both innate and adaptive immune responses were required to recapitulate all the observed dose-dependent relationships.[117] New ZIKV studies exploring dose-dependent relationships might thus provide insights into the type of immune responses that control plasma viral load.

5 | MODELING ANTIVIRAL DRUG TREATMENT

Mathematical modeling of viral dynamics allows for exploration of various therapeutic options and has provided insight into antiviral efficacy in HIV and HCV.[103,118] The effect of an antiviral drug can be modeled by modulating the appropriate rate parameter with a term $(1-\varepsilon)$, where ε is the efficacy of the drug. HIV reverse transcriptase inhibitors act to prevent viral infection and have been incorporated into models as a reduction in the viral infection term: $(1-\varepsilon)\beta VT$, in both the target cell and infected cell ODEs.[119] HCV polymerase inhibitors, such as sofosbuvir,[120] have been modeled via restriction of viral production from infected cells: $(1-\varepsilon)pI_2$ in the ODE for free virus.[120] HIV protease inhibitors, such as ritonavir, result in production of viral particles that are not infectious, and the approach to modeling this antiviral action has been to introduce an additional ODE representing non-infectious virus V_N[19]

$$\begin{aligned}\frac{dV}{dt} &= (1-\varepsilon)pI_2 - cV\\ \frac{dV_N}{dt} &= \varepsilon pI_2 - cV_N\end{aligned} \tag{19}$$

where the total virus $V + V_N$ describes the observed viral RNA.

If there is no detailed information about the efficacy of potential antiviral therapies, modeling can predict the efficacy required in order to restrict viremia by a particular amount. In particular, the reproductive ratio under any of these 3 antiviral drug models becomes $\hat{R}_0 = (1-\varepsilon)R_0$, and as such the drug efficacy required to reduce this to below 1 and therefore prevent viral infection taking hold is $\varepsilon > \varepsilon_c = 1 - \frac{1}{R_0}$, where ε_c is called the critical efficacy.[121]

Much effort has been applied to discovering antiviral drugs active against ZIKV.[122,123] One promising candidate, BCX4430 now called galidesivir, has shown potent activity in ZIKV-infected NHPs.[124] For many potential drugs the EC_{50}, that is, the concentration required to provide 50% inhibition of viral replication, has been measured in vitro. For a given drug concentration C, the drug efficacy could be assumed to be $\varepsilon = C/(C+EC_{50})$, or more generally by an expression including a Hill coefficient n,[125] $\varepsilon = C^n/(C^n + EC_{50}{}^n)$. Using either of these equations, the effect of different constant drug concentrations on the viral load dynamics can be assessed. Applying this approach to ZIKV,[30] we found that for a drug reducing the viral production rate with efficacy $\varepsilon = C/(C+EC_{50})$ under the target cell limited model with an exponentially distributed eclipse phase (Equation 2), the time to undetectable viral load and the total viral burden is increased at low C/EC_{50} ratios and only when this ratio exceeds a particular threshold is there improvement in these two measures above the case in which no drug is applied (Figure 7). The concentration threshold above which drug reduces viral burden depends on the viral dynamics parameters. This increased viral burden at low drug concentrations is due to the slower infection of target cells, which prolongs the viral infection (Figure 7A). While this result is worrisome, it may not be realistic in circumstances where an immune response develops and controls viremia, or for effective drugs where concentrations well above these thresholds are attained. Also, presuming a constant drug concentration applied from the time of infection is not realistic in any clinical setting. A more comprehensive approach to modeling the effect of an antiviral drug is to adopt a time-varying drug concentration, which then leads to a model incorporating both pharmacokinetics and pharmacodynamics, as has been done for the treatment of other viral infections.[29,126,127]

Analysis of ZIKV dynamics during antiviral therapy can provide insight into therapy efficacy, but could also provide further evidence regarding immune control. If target cell limitation is the key component of immune control, we might expect a delay in viremia but not reduction in total viral shedding on antiviral therapy. However, if antiviral therapy is seen to both delay and reduce viremia then this suggests an immune response is key to controlling viremia and as such a model incorporating an immune mechanism, as described early, would be required to fully describe the observed data.

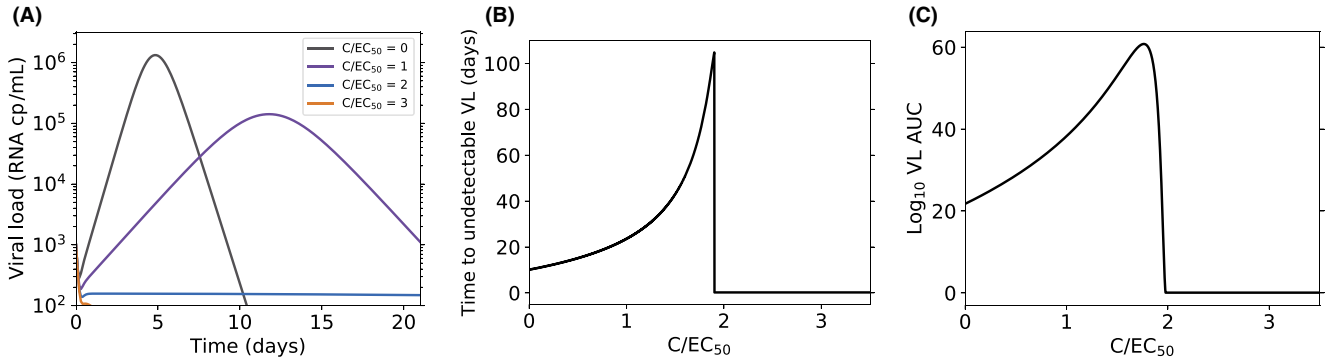

Figure 7. Predicted effects of antiviral therapy. With an antiviral drug reducing the viral production rate in the target cell-limited model (Equation 2) with an efficacy $\varepsilon = C/(C+EC_{50})$, (A) the predicted viral kinetics at different ratios of drug concentration C to drug EC_{50}, (B) the predicted time to undetectable viral load and (C) the predicted total viral burden measured as the $\log_{10}$ viral load area under the curve (AUC) as a function of the C/EC_{50} ratio. Viral dynamic parameters R_0 = 3 per day, k = 4 per day, δ = 3.5 per day, p = 1000 per day, c = 10 per day, $T(0) = 10^5$ per mL, $V(0) = 10^3$ per mL, limit of detection = 200 RNA copies per mL

6 | CONCLUSION

There is much to still be understood about ZIKV infection, including the kinetics of viral growth and spread within an individual and the key mechanisms of immune control. Further experimental data, from in vitro studies and NHP studies as well as in vivo observations from infected patients, when combined with mathematical modeling will be of vital importance in increasing our understanding of ZIKV infection. Here, we have discussed the modeling approaches that have been taken to provide insight into viral dynamics, immune control, and antiviral efficacy.

ACKNOWLEDGEMENTS

Portions of this work were done under the auspices of the US Department of Energy under Contract DE-AC52-06NA25396. This work was also supported by NIH Grants R01-AI078881, R01-OD0110955, and R01-AI028433 (to A.S.P.). We thank Jeremie Guedj and Ruy Ribeiro for helpful discussions and comments.

CONFLICT OF I NTEREST

The authors declare no conflicts of interest.

ORCID

Alan S Perelson http://orcid.org/0000-0002-2455-0002

REFERENCES

1. Dick GWA, Kitchen SF, Haddow AJ. Zika virus (I). Isolations and serological specificity. *Trans R Soc Trop Med Hyg*. 1952;46:509-520. https://doi.org/10.1016/0035-9203(52)90042-4.
2. Duffy MR, Chen T-H, Hancock WT, et al. Zika virus outbreak on Yap Island, Federated States of Micronesia. *N Engl J Med*. 2009;360:2536-2543. https://doi.org/10.1056/NEJMoa0805715.
3. Campos GS, Bandeira AC, Sardi SI. Zika virus outbreak, Bahia, Brazil. *Emerg Infect Dis*. 2015;21:1885-1886. https://doi.org/10.3201/eid2110.150847.
4. Brasil P, Calvet GA, Siqueira AM, et al. Zika virus outbreak in Rio de Janeiro, Brazil: clinical characterization, epidemiological and virological aspects. *PLoS Negl Trop Dis*. 2016;10:e0004636. https://doi.org/10.1371/journal.pntd.0004636.
5. Cao-Lormeau V-M, Blake A, Mons S, et al. Guillain-Barré syndrome outbreak associated with Zika virus infection in French Polynesia: a case-control study. *Lancet*. 2016;387:1531-1539. https://doi.org/10.1016/S0140-6736(16)00562-6.
6. Ventura CV, Maia M, Bravo-Filho V, Góis AL, Belfort R. Zika virus in Brazil and macular atrophy in a child with microcephaly. *Lancet*. 2016;387:228. https://doi.org/10.1016/S0140-6736(16)00006-4.
7. Joguet G, Mansuy J, Matusali G, et al. Effect of acute Zika virus infection on sperm and virus clearance in body fluids: a prospective observational study. *Lancet Infect Dis*. 2017;17:1200-1208. https://doi.org/10.1016/S1473-3099(17)30444-9.
8. Paz-Bailey G, Rosenberg ES, Doyle K, et al. Persistence of Zika virus in body fluids — preliminary report. *N Engl J Med*. 2017. https://doi.org/10.1056/NEJMoa1613108.
9. Jeong YE, Cha G-W, Cho JE, Lee EJ, Jee Y, Lee W-J. Viral and serological kinetics in Zika virus-infected patients in South Korea. *Virol J*. 2017;14:70. https://doi.org/10.1186/s12985-017-0740-6.
10. Mead PS, Duggal NK, Hook SA, et al. Zika virus shedding in semen of symptomatic infected men. *N Engl J Med*. 2018;378:1377-1385. https://doi.org/10.1056/NEJMoa1711038.
11. Dupont-Rouzeyrol M, Biron A, O'Connor O, Huguon E, Descloux E. Infectious Zika viral particles in breastmilk. *Lancet*. 2016;387:1051. https://doi.org/10.1016/S0140-6736(16)00624-3.
12. Papa MP, Meuren LM, Coelho SVA, et al. Zika virus infects, activates, and crosses brain microvascular endothelial cells, without barrier disruption. *Front Microbiol*. 2017;8:2557. https://doi.org/10.3389/fmicb.2017.02557.
13. Mladinich MC, Schwedes J, Mackow ER. Zika virus persistently infects and is basolaterally released from primary human brain microvascular endothelial cells. *MBio*. 2017;8:e00952-17. https://doi.org/10.1128/mbio.00952-17.
14. Richard AS, Shim B-S, Kwon Y-C, et al. AXL-dependent infection of human fetal endothelial cells distinguishes Zika virus from other pathogenic flaviviruses. *Proc Natl Acad Sci USA*. 2017;114:2024-2029. https://doi.org/10.1073/pnas.1620558114.
15. Sheridan MA, Yunusov D, Balaraman V, et al. Vulnerability of primitive human placental trophoblast to Zika virus. *Proc Natl Acad Sci USA*. 2017;114:E1587-E1596. https://doi.org/10.1073/pnas.1616097114.
16. Petitt M, Tabata T, Puerta-Guardo H, Harris E, Pereira L. Zika virus infection of first-trimester human placentas: utility of an explant

model of replication to evaluate correlates of immune protection ex vivo. *Curr Opin Virol*. 2017;27:48-56. https://doi.org/10.1016/j.coviro.2017.11.008.
17. Barouch DH, Thomas SJ, Michael NL. Prospects for a Zika virus vaccine. *Immunity*. 2017;46:176-182. https://doi.org/10.1016/j.immuni.2017.02.005.
18. Blackman MA, Kim I-J, Lin J-S, Thomas SJ. Challenges of vaccine development for Zika virus. *Viral Immunol*. 2018;31:117-123. https://doi.org/10.1089/vim.2017.0145.
19. Perelson AS, Neumann AU, Markowitz M, Leonard JM, Ho DD. HIV-1 dynamics in vivo: virion clearance rate, infected cell lifespan, and viral generation time. *Science*. 1996;271:1582-1586. https://doi.org/10.1126/science.271.5255.1582.
20. Neumann AU, Lam NP, Dahari H, et al. Hepatitis C viral dynamics in vivo and the antiviral efficacy of interferon-alpha therapy. *Science*. 1998;282:103-107. https://doi.org/10.1126/science.282.5386.103.
21. Perelson AS. Modelling viral and immune system dynamics. *Nat Rev Immunol*. 2002;2:28-36. https://doi.org/10.1038/nri700.
22. Baccam P, Beauchemin C, Macken CA, Hayden FG, Perelson AS. Kinetics of influenza A virus infection in humans. *J Virol*. 2006;80:7590-7599. https://doi.org/10.1128/JVI.01623-05.
23. Beauchemin CA, Handel A. A review of mathematical models of influenza A infections within a host or cell culture: lessons learned and challenges ahead. *BMC Public Health*. 2011;11(Suppl 1):S7. https://doi.org/10.1186/1471-2458-11-S1-S7.
24. Smith AM, Perelson AS. Influenza A virus infection kinetics: quantitative data and models. *Wiley Interdiscip Rev Syst Biol Med*. 2011;3:429-445. https://doi.org/10.1002/wsbm.129.
25. Banerjee S, Guedj J, Ribeiro RM, Moses M, Perelson AS. Estimating biologically relevant parameters under uncertainty for experimental within-host murine West Nile virus infection. *J R Soc Interface*. 2016;13:20160130. https://doi.org/10.1098/rsif.2016.0130.
26. Banerjee S, Perelson AS, Moses M. Modelling the effects of phylogeny and body size on within-host pathogen replication and immune response. *J R Soc Interface*. 2017;14. https://doi.org/10.1098/rsif.2017.0479.
27. Ben-Shachar R, Koelle K. Minimal within-host dengue models highlight the specific roles of the immune response in primary and secondary dengue infections. *J R Soc Interface*. 2014;12:20140886. https://doi.org/10.1098/rsif.2014.0886.
28. Clapham HE, Tricou V, Van Vinh Chau N, Simmons CP, Ferguson NM. Within-host viral dynamics of dengue serotype 1 infection. *J R Soc Interface*. 2014;11:20140094. https://doi.org/10.1098/rsif.2014.0094.
29. Madelain V, Oestereich L, Graw F, et al. Ebola virus dynamics in mice treated with favipiravir. *Antiviral Res*. 2015;123:70-77. https://doi.org/10.1016/j.antiviral.2015.08.015.
30. Best K, Guedj J, Madelain V, et al. Zika plasma viral dynamics in nonhuman primates provides insights into early infection and antiviral strategies. *Proc Natl Acad Sci USA*. 2017;114:8847-8852. https://doi.org/10.1073/pnas.1704011114.
31. Barzon L, Percivalle E, Pacenti M, et al. Virus and antibody dynamics in travelers with acute Zika virus infection. *Clin Infect Dis*. 2018;66:1173-1180. https://doi.org/10.1093/cid/cix967.
32. Suy A, Sulleiro E, Rodó C, et al. Prolonged Zika virus viremia during pregnancy. *N Engl J Med*. 2016;375:2611-2613. https://doi.org/10.1056/NEJMc1607580.
33. Lazear HM, Govero J, Smith AM, et al. A mouse model of Zika virus pathogenesis. *Cell Host Microbe*. 2016;19:720-730. https://doi.org/10.1016/j.chom.2016.03.010.
34. Estes JD, Wong SW, Brenchley JM. Nonhuman primate models of human viral infections. *Nat Rev Immunol*. 2018. https://doi.org/10.1038/s41577-018-0005-7.
35. Osuna CE, Whitney JB. Nonhuman primate models of Zika virus infection, immunity, and therapeutic development. *J Infect Dis*. 2017;216(S10):S928-S934. https://doi.org/10.1093/infdis/jix540.
36. Newman C, Friedrich TC, O'Connor DH. Macaque monkeys in Zika virus research: 1947–present. *Curr Opin Virol*. 2017;25:34-40. https://doi.org/10.1016/j.coviro.2017.06.011.
37. Martinot AJ, Abbink P, Afacan O, et al. Fetal neuropathology in Zika virus-infected pregnant female rhesus monkeys. *Cell*. 2018;173:1-12. https://doi.org/10.1016/j.cell.2018.03.019.
38. Simonin Y, van Riel D, Van de Perre P, Rockx B, Salinas S. Differential virulence between Asian and African lineages of Zika virus. *PLoS Negl Trop Dis*. 2017;11:e0005821. https://doi.org/10.1371/journal.pntd.0005821.
39. Hamel R, Dejarnac O, Wichit S, et al. Biology of Zika virus infection in human skin cells. *J Virol*. 2015;89:8880-8896. https://doi.org/10.1128/JVI.00354-15.
40. Retallack H, Di Lullo E, Arias C, et al. Zika virus cell tropism in the developing human brain and inhibition by azithromycin. *Proc Natl Acad Sci USA*. 2016;113:14408-14413. https://doi.org/10.1073/pnas.1618029113.
41. Quicke KM, Bowen JR, Johnson EL, et al. Zika virus infects human placental macrophages. *Cell Host Microbe*. 2016;20:83-90. https://doi.org/10.1016/j.chom.2016.05.015.
42. El Costa H, Gouilly J, Mansuy J-M, et al. Zika virus reveals broad tissue and cell tropism during the first trimester of pregnancy. *Sci Rep*. 2016;6:35296. https://doi.org/10.1038/srep35296.
43. Aagaard KM, Lahon A, Suter MA, et al. Primary human placental trophoblasts are permissive for Zika virus (ZIKV) replication. *Sci Rep*. 2017;7:41389. https://doi.org/10.1038/srep41389.
44. Spencer JL, Lahon A, Tran LL, et al. Replication of Zika virus in human prostate cells: a potential source of sexually transmitted virus. *J Infect Dis*. 2018;217:538-547. https://doi.org/10.1093/infdis/jix436.
45. Meertens L, Labeau A, Dejarnac O, et al. Axl mediates Zika virus entry in human glial cells and modulates innate immune responses. *Cell Rep*. 2017;18:324-333. https://doi.org/10.1016/j.celrep.2016.12.045.
46. Coffey LL, Pesavento PA, Keesler RI, et al. Zika virus tissue and blood compartmentalization in acute infection of rhesus macaques. *PLoS ONE*. 2017;12:e0171148. https://doi.org/10.1371/journal.pone.0171148.
47. Mohr EL, Block LN, Newman CM, et al. Ocular and uteroplacental pathology in a macaque pregnancy with congenital Zika virus infection. *PLoS ONE*. 2018;13:e0190617. https://doi.org/10.1371/journal.pone.0190617.
48. Hirsch AJ, Roberts VHJ, Grigsby PL, et al. Zika virus infection in pregnant rhesus macaques causes placental dysfunction and immunopathology. *Nat Commun*. 2018;9:263. https://doi.org/10.1038/s41467-017-02499-9.
49. Nguyen SM, Antony KM, Dudley DM, et al. Highly efficient maternal-fetal Zika virus transmission in pregnant rhesus macaques. *PLoS Pathog*. 2017;13:e1006378. https://doi.org/10.1371/journal.ppat.1006378.
50. Seferovic M, Martín CS-S, Tardif SD, et al. Experimental Zika virus infection in the pregnant common marmoset induces spontaneous fetal loss and neurodevelopmental abnormalities. *Sci Rep*. 2018;8:6851. https://doi.org/10.1038/s41598-018-25205-1.
51. Dudley DM, Newman CM, Lalli J, et al. Infection via mosquito bite alters Zika virus tissue tropism and replication kinetics in rhesus macaques. *Nat Commun*. 2017;8:2096. https://doi.org/10.1038/s41467-017-02222-8.
52. Newman CM, Dudley DM, Aliota MT, et al. Oropharyngeal mucosal transmission of Zika virus in rhesus macaques. *Nat Commun*. 2017;8:169. https://doi.org/10.1038/s41467-017-00246-8.

53. Carroll T, Lo M, Lanteri M, et al. Zika virus preferentially replicates in the female reproductive tract after vaginal inoculation of rhesus macaques. *PLoS Pathog*. 2017;13:1-23. https://doi.org/10.1371/journal.ppat.1006537.
54. Haddow AD, Nalca A, Rossi FD, et al. High infection rates for adult macaques after intravaginal or intrarectal inoculation with Zika virus. *Emerg Infect Dis*. 2017;23:1274-1281. https://doi.org/10.3201/eid2308.170036.
55. Souza BSF, Sampaio GLA, Pereira CS, et al. Zika virus infection induces mitosis abnormalities and apoptotic cell death of human neural progenitor cells. *Sci Rep*. 2016;6:39775. https://doi.org/10.1038/srep39775.
56. Alpuche-Lazcano S, McCullogh C, Del Corpo O, et al. Higher cytopathic effects of a Zika virus Brazilian isolate from Bahia compared to a Canadian-imported Thai strain. *Viruses*. 2018;10:53. https://doi.org/10.3390/v10020053.
57. Di Mascio M, Dornadula G, Zhang H, et al. In a subset of subjects on highly active antiretroviral therapy, human immunodeficiency virus Type 1 RNA in plasma decays from 50 to <5 copies per milliliter, with a half-life of 6 months. *J Virol*. 2003;77:2271-2275. https://doi.org/10.1128/JVI.77.3.2271-2275.2003.
58. Lavielle M. *Mixed Effects Models for the Population Approach*. Chapman and Hall/CRC Biostatistics Series. Boca Raton, FL: Chapman and Hall/CRC; 2015.
59. Ribeiro RM, Qin L, Chavez LL, Li D, Self SG, Perelson AS. Estimation of the initial viral growth rate and basic reproductive number during acute HIV-1 infection. *J Virol*. 2010;84:6096-6102. https://doi.org/10.1128/JVI.00127-10.
60. Snoeck E, Chanu P, Lavielle M, et al. A comprehensive hepatitis C viral kinetic model explaining cure. *Clin Pharmacol Ther*. 2010;87:706-713. https://doi.org/10.1038/clpt.2010.35.
61. Raftery AE. Bayesian model selection in social research. *Sociol Methodol*. 1995;25:111-163.
62. Saá P, Ph D, Proctor M, et al. Investigational testing for Zika virus among U.S. blood donors. *N Engl J Med*. 2018;378:1837-1841. https://doi.org/10.1056/NEJMoa1714977.
63. Miao H, Xia X, Perelson AS, Wu H. On identifiability of nonlinear ODE models and applications in viral dynamics. *SIAM Rev*. 2011;53:3-39. https://doi.org/10.1137/090757009.
64. Stafford MA, Corey L, Cao Y, Daar ES, Ho DD, Perelson AS. Modeling plasma virus concentration during primary HIV infection. *J Theor Biol*. 2000;203:285-301. https://doi.org/10.1006/jtbi.2000.1076.
65. Dudley DM, Aliota MT, Mohr EL, et al. A rhesus macaque model of Asian-lineage Zika virus infection. *Nat Commun*. 2016;7:12204. https://doi.org/10.1038/ncomms12204.
66. Guedj J, Thiébaut R, Commenges D. Practical identifiability of HIV dynamics models. *Bull Math Biol*. 2007;69:2493-2513. https://doi.org/10.1007/s11538-007-9228-7.
67. Nguyen VK, Klawonn F, Mikolajczyk R, Hernandez-Vargas EA. Analysis of practical identifiability of a viral infection model. *PLoS ONE*. 2016;11:1-16. https://doi.org/10.1371/journal.pone.0167568.
68. Smith AM, Adler FR, Ribeiro RM, et al. Kinetics of coinfection with influenza A virus and Streptococcus pneumoniae. *PLoS Pathog*. 2013;9:e1003238. https://doi.org/10.1371/journal.ppat.1003238.
69. Smith AM, Smith AP. A critical, nonlinear threshold dictates bacterial invasion and initial kinetics during influenza. *Sci Rep*. 2016;6:38703. https://doi.org/10.1038/srep38703.
70. Bai F, Huff KES, Allen LJS. The effect of delay in viral production in within-host models during early infection. *J Biol Dyn*. 2018. https://doi.org/10.1080/17513758.2018.1498984
71. Sacha JB, Chung C, Rakasz EG, et al. Gag-specific CD8+ T lymphocytes recognize infected cells before AIDS-virus integration and viral protein expression. *J Immunol*. 2007;178:2746-2754. https://doi.org/10.4049/jimmunol.178.5.2746.
72. Holder BP, Beauchemin CAA. Exploring the effect of biological delays in kinetic models of influenza within a host or cell culture. *BMC Public Health*. 2011;11(Suppl 1):S10. https://doi.org/10.1186/1471-2458-11-S1-S10.
73. Kakizoe Y, Nakaoka S, Beauchemin CAA, et al. A method to determine the duration of the eclipse phase for in vitro infection with a highly pathogenic SHIV strain. *Sci Rep*. 2015;5:10371. https://doi.org/10.1038/srep10371.
74. Mittler JE, Sulzer B, Neumann AU, Perelson AS. Influence of delayed viral production on viral dynamics in HIV-1 infected patients. *Math Biosci*. 1998;152:143-163. https://doi.org/10.1016/S0025-5564(98)10027-5.
75. Pinilla LT, Holder BP, Abed Y, Boivin G, Beauchemin CAA. The H275Y neuraminidase mutation of the pandemic A/H1N1 influenza virus lengthens the eclipse phase and reduces viral output of infected cells, potentially compromising fitness in ferrets. *J Virol*. 2012;86:10651-10660. https://doi.org/10.1128/JVI.07244-11.
76. Gonzàlez-Parra G, De Ridder F, Huntjens D, Roymans D, Ispas G, Dobrovolny HM. A comparison of RSV and influenza in vitro kinetic parameters reveals differences in infecting time. *PLoS ONE*. 2018;13:e0192645. https://doi.org/10.1371/journal.pone.0192645.
77. Möhler L, Flockerzi D, Sann H, Reichl U. Mathematical model of influenza A virus production in large-scale microcarrier culture. *Biotechnol Bioeng*. 2005;90:46-58. https://doi.org/10.1002/bit.20363.
78. Herz AV, Bonhoeffer S, Anderson RM, May RM, Nowak MA. Viral dynamics in vivo: limitations on estimates of intracellular delay and virus decay. *Proc Natl Acad Sci USA*. 1996;93:7247-7251. https://doi.org/10.1073/pnas.93.14.7247.
79. Mitchell H, Levin D, Forrest S, et al. Higher level of replication efficiency of 2009 (H1N1) pandemic influenza virus than those of seasonal and avian strains: kinetics from epithelial cell culture and computational modeling. *J Virol*. 2011;85:1125-1135. https://doi.org/10.1128/JVI.01722-10.
80. Li S, Armstrong N, Zhao H, et al. Zika virus fatally infects wild type neonatal mice and replicates in central nervous system. *Viruses*. 2018;10:49. https://doi.org/10.3390/v10010049.
81. Grant A, Ponia SS, Tripathi S, et al. Zika virus targets human STAT2 to inhibit type I interferon signaling. *Cell Host Microbe*. 2016;19:882-890. https://doi.org/10.1016/j.chom.2016.05.009.
82. Glasner A, Oiknine-Djian E, Weisblum Y, et al. Zika virus escapes NK cell detection by upregulating major histocompatibility complex class I molecules. *J Virol*. 2017;91:e00785-17. https://doi.org/10.1128/JVI.00785-17.
83. Priyamvada L, Suthar MS, Ahmed R, Wrammert J. Humoral immune responses against Zika virus infection and the importance of preexisting flavivirus immunity. *J Infect Dis*. 2017;216(S10):S906-S911. https://doi.org/10.1093/infdis/jix513.
84. El Silveira V, Rogers KA, Amancha P, et al. Immune cell dynamics in rhesus macaques infected with a Brazilian strain of Zika virus. *J Immunol*. 2017;199:1003-1011. https://doi.org/10.4049/jimmunol.1700256.
85. Aliota MT, Dudley DM, Newman CM, et al. Heterologous protection against Asian Zika virus challenge in rhesus macaques. *PLoS Negl Trop Dis*. 2016;10:e0005168. https://doi.org/10.1371/journal.pntd.0005168.
86. Osuna CE, Lim S-Y, Deleage C, et al. Zika viral dynamics and shedding in rhesus and cynomolgus macaques. *Nat Med*. 2016;22:1448-1455. https://doi.org/10.1038/nm.4206.
87. Chiu CY, Sánchez-San Martín C, Bouquet J, et al. Experimental Zika virus inoculation in a new world monkey model reproduces key features of the human infection. *Sci Rep*. 2017;7:17126. https://doi.org/10.1038/s41598-017-17067-w.

88. Lai L, Rouphael N, Xu Y, et al. Innate, T-, and B-cell responses in acute human Zika patients. *Clin Infect Dis*. 2018;66:1-10. https://doi.org/10.1093/cid/cix732.
89. Priyamvada L, Quicke KM, Hudson WH, et al. Human antibody responses after dengue virus infection are highly cross-reactive to Zika virus. *Proc Natl Acad Sci USA*. 2016;113:7852-7857. https://doi.org/10.1073/pnas.1607931113.
90. Yu L, Wang R, Gao F, et al. Delineating antibody recognition against Zika virus during natural infection. *JCI Insight*. 2017;2:1-16. https://doi.org/10.1172/jci.insight.93042.
91. Katzelnick LC, Gresh L, Halloran ME, et al. Antibody-dependent enhancement of severe dengue disease in humans. *Science*. 2017;358:929-932. https://doi.org/10.1126/science.aan6836.
92. Dejnirattisai W, Supasa P, Wongwiwat W, et al. Dengue virus sero-cross-reactivity drives antibody-dependent enhancement of infection with Zika virus. *Nat Immunol*. 2016;17:1102-1108. https://doi.org/10.1038/ni.3515.
93. McCracken MK, Gromowski GD, Friberg HL, et al. Impact of prior flavivirus immunity on Zika virus infection in rhesus macaques. *PLoS Pathog*. 2017;13:e1006487. https://doi.org/10.1371/journal.ppat.1006487.
94. Pantoja P, Pérez-Guzmán EX, Rodríguez IV, et al. Zika virus pathogenesis in rhesus macaques is unaffected by pre-existing immunity to dengue virus. *Nat Commun*. 2017;8:15674. https://doi.org/10.1038/ncomms15674.
95. Fernandez E, Dejnirattisai W, Cao B, et al. Human antibodies to the dengue virus E-dimer epitope have therapeutic activity against Zika virus infection. *Nat Immunol*. 2017;18:1261-1269. https://doi.org/10.1038/ni.3849.
96. Huang H, Li S, Zhang Y, et al. CD8+ T cell immune response in immunocompetent mice during Zika virus infection. *J Virol*. 2017;91:e00900-17. https://doi.org/10.1128/JVI.00900-17.
97. Elong Ngono A, Vizcarra EA, Tang WW, et al. Mapping and role of the CD8+ T cell response during primary Zika virus infection in mice. *Cell Host Microbe*. 2017;21:35-46. https://doi.org/10.1016/j.chom.2016.12.010.
98. García-Sastre A, Durbin RK, Zheng H, et al. The role of interferon in influenza virus tissue tropism. *J Virol*. 1998;72:8550-8558.
99. Schoggins JW, Rice CM. Interferon-stimulated genes and their antiviral effector functions. *Curr Opin Virol*. 2011;1:519-525. https://doi.org/10.1016/j.coviro.2011.10.008.
100. Pawelek KA, Huynh GT, Quinlivan M, Cullinane A, Rong L, Perelson AS. Modeling within-host dynamics of influenza virus infection including immune responses. *PLoS Comput Biol*. 2012;8:e1002588. https://doi.org/10.1371/journal.pcbi.1002588.
101. Saenz RA, Quinlivan M, Elton D, et al. Dynamics of influenza virus infection and pathology. *J Virol*. 2010;84:3974-3983. https://doi.org/10.1128/JVI.02078-09.
102. Dixit NM, Layden-Almer JE, Layden TJ, Perelson AS. Modelling how ribavirin improves interferon response rates in hepatitis C virus infection. *Nature*. 2004;432:922-924. https://doi.org/10.1038/nature03153.
103. Perelson AS, Guedj J. Modelling hepatitis C therapy—predicting effects of treatment. *Nat Rev Gastroenterol Hepatol*. 2015;12:437-445. https://doi.org/10.1038/nrgastro.2015.97.
104. Handel A, Longini IM, Antia R. Towards a quantitative understanding of the within-host dynamics of influenza A infections. *J R Soc Interface*. 2010;7:35-47. https://doi.org/10.1098/rsif.2009.0067.
105. Conway JM, Perelson AS. Post-treatment control of HIV infection. *Proc Natl Acad Sci USA*. 2015;112:5467-5472. https://doi.org/10.1073/pnas.1419162112.
106. De Boer RJ, Perelson AS. Target cell limited and immune control models of HIV infection: a comparison. *J Theor Biol*. 1998;190:201-214. https://doi.org/10.1006/jtbi.1997.0548.
107. Johnson PLF, Kochin BF, McAfee MS, et al. Vaccination alters the balance between protective immunity, exhaustion, escape, and death in chronic infections. *J Virol*. 2011;85:5565-5570. https://doi.org/10.1128/JVI.00166-11.
108. De Boer RJ, Homann D, Perelson AS. Different dynamics of CD4+ and CD8+ T cell responses during and after acute lymphocytic choriomeningitis virus infection. *J Immunol*. 2003;171:3928-3935. https://doi.org/10.4049/jimmunol.171.8.3928.
109. De Boer RJ, Oprea M, Antia R, Murali-Krishna K, Ahmed R, Perelson AS. Recruitment times, proliferation, and apoptosis rates during the CD8+ T-Cell response to lymphocytic choriomeningitis virus. *J Virol*. 2001;75:10663-10669. https://doi.org/10.1128/JVI.75.22.10663-10669.2001.
110. Miao H, Hollenbaugh JA, Zand MS, et al. Quantifying the early immune response and adaptive immune response kinetics in mice infected with influenza A virus. *J Virol*. 2010;84:6687-6698. https://doi.org/10.1128/JVI.00266-10.
111. Perelson AS, Goldstein B, Rocklin S. Optimal strategies in immunology III. The IgM-IgG switch. *J Math Biol*. 1980;10:209-256.
112. Ciupe SM, Ribeiro RM, Perelson AS. Antibody responses during hepatitis B viral infection. *PLoS Comput Biol*. 2014;10:e1003730. https://doi.org/10.1371/journal.pcbi.1003730.
113. Smith DJ, Forrest S, Ackley DH, Perelson AS. Variable efficacy of repeated annual influenza vaccination. *Proc Natl Acad Sci*. 1999;96:14001-14006. https://doi.org/10.1073/pnas.96.24.14001.
114. Tomaras GD, Yates NL, Liu P, et al. Initial B-Cell responses to transmitted human immunodeficiency virus type 1: virion-binding immunoglobulin M (IgM) and IgG antibodies followed by plasma anti-gp41 antibodies with ineffective control of initial viremia. *J Virol*. 2008;82:12449-12463. https://doi.org/10.1128/JVI.01708-08.
115. Dutra HLC, Rocha MN, Dias FBS, Mansur SB, Caragata EP, Moreira LA. Wolbachia blocks currently circulating Zika virus isolates in Brazilian *Aedes aegypti* mosquitoes. *Cell Host Microbe*. 2016;19:771-774. https://doi.org/10.1016/j.chom.2016.04.021.
116. Aid M, Abbink P, Larocca RA, et al. Zika virus persistence in the central nervous system and lymph nodes of rhesus monkeys. *Cell*. 2017;169(610–620):e14. https://doi.org/10.1016/j.cell.2017.04.008.
117. Li Y, Handel A. Modeling inoculum dose dependent patterns of acute virus infections. *J Theor Biol*. 2014;347:63-73. https://doi.org/10.1016/j.jtbi.2014.01.008.
118. Perelson AS, Ribeiro RM. Estimating drug efficacy and viral dynamic parameters: HIV and HCV. *Stat Med*. 2008;27:4647-4657. https://doi.org/10.1002/sim.3116.
119. Perelson AS, Nelson PW. Mathematical analysis of HIV-1 dynamics in vivo. *SIAM Rev*. 1999;41:3-44. https://doi.org/10.1137/S0036144598335107.
120. Guedj J, Pang PS, Denning J, et al. Analysis of the hepatitis C viral kinetics during administration of two nucleotide analogues: sofosbuvir (GS-7977) and GS-0938. *Antivir Ther*. 2014;19:211-220. https://doi.org/10.3851/IMP2733.
121. Dahari H, Lo A, Ribeiro RM, Perelson AS. Modeling hepatitis C virus dynamics: liver regeneration and critical drug efficacy. *J Theor Biol*. 2007;247:371-381. https://doi.org/10.1016/j.jtbi.2007.03.006.
122. Saiz J, Martín-Acebes MA. The race to find antivirals for Zika virus. *Antimicrob Agents Chemother*. 2017;61:e00411-17. https://doi.org/10.1128/AAC.00411-17.
123. Munjal A, Khandia R, Dhama K, et al. Advances in developing therapies to combat Zika virus: current knowledge and future perspectives. *Front Microbiol*. 2017;8:1469. https://doi.org/10.3389/fmicb.2017.01469.
124. Lim S-Y, Osuna C, Taylor R, et al. BCX4430, a broad-spectrum adenosine analog direct-acting antiviral drug, abrogates viremia in rhesus macaques challenged with Zika virus. https://idsa.confex.

com/idsa/2016/webprogram/Paper60907.html. Accessed July 05, 2018.
125. Shen L, Peterson S, Sedaghat AR, et al. Dose-response curve slope sets class-specific limits on inhibitory potential of anti-HIV drugs. *Nat Med*. 2008;14:762-766. https://doi.org/10.1038/nm1777.
126. Wu H, Huang Y, Acosta EP, et al. Pharmacodynamics of antiretroviral agents in HIV-1 infected patients: using viral dynamic models that incorporate drug susceptibility and adherence. *J Pharmacokinet Pharmacodyn*. 2006;33:399-419. https://doi.org/10.1007/s10928-006-9006-4.
127. Talal AH, Ribeiro RM, Powers KA, et al. Pharmacodynamics of PEG-IFNα differentiate HIV/HCV coinfected sustained virological responders from nonresponders. *Hepatology*. 2006;43:943-953. https://doi.org/10.1002/hep.21136.
128. Aliota MT, Dudley DM, Newman CM, et al. Molecularly barcoded Zika virus libraries to probe in vivo evolutionary dynamics. *PLoS Pathog*. 2018;14:e1006964. https://doi.org/10.1371/journal.ppat.1006964.

How to cite this article: Best K, Perelson AS. Mathematical modeling of within-host Zika virus dynamics. *Immunol Rev*. 2018;285:81–96. https://doi.org/10.1111/imr.12687